

Acoustic emission and energy dissipation during front propagation in a stress-driven martensitic transition

Erell Bonnot, Eduard Vives, Lluís Mañosa, and Antoni Planes

Departament d'Estructura i Constituents de la Matèria, Facultat de Física, Universitat de Barcelona, Diagonal 647, E-08028 Barcelona, Catalonia

Ricardo Romero

IFIMAT, Universidad del Centro de la Provincia de Buenos Aires and Comisión de Investigaciones Científicas de la Provincia de Buenos Aires, Pinto 399, 7000 Tandil, Argentina

(Received 15 April 2008; revised manuscript received 24 June 2008; published 5 September 2008)

In the present paper, by using a specially designed experiment, we analyze the relationship between the acoustic emission and the deformation resulting from front propagation during a stress-induced transition from cubic to a single-variant martensite in a Cu-Zn-Al single crystal. The front propagates by nucleation and growing needle domains parallel to the parent martensitic interface. A good correlation between the acoustic emission activity and front velocity is obtained. By using a phenomenological model, we discuss the relation between such acoustic activity and the dissipated energy during the process. Results suggest that the acoustic emission has its origin in the interaction of needle domains and dislocations.

DOI: [10.1103/PhysRevB.78.094104](https://doi.org/10.1103/PhysRevB.78.094104)

PACS number(s): 81.30.Kf, 64.60.av, 61.72.Hh

I. INTRODUCTION

Acoustic waves are emitted during many externally stimulated solid-state processes which occur at scales ranging from nanometers to micrometers. These acoustic waves propagate through the solid and can be detected by means of suitable sensors giving rise to the so-called acoustic emission (AE).¹ AE has been reported in plasticity-related phenomena such as dislocation dynamics,^{2,3} microcrack propagation,⁴ and first-order phase transitions taking place in (multi)ferroic materials.^{5,6} Detection of AE reveals an intermittent and jerky character of the dynamics in all these phenomena. Usually an external field is responsible for the modification of the internal distribution of strains due to induced local (micro/nano) displacements which are at the origin of the generated acoustic waves. Therefore, it is commonly assumed that AE provides basic information related to energy dissipation mechanisms of the studied process.

In first-order phase transitions local displacements are directly related to the transition mechanism when strain is the primary order parameter as in the case of ferroelastic or martensitic transitions or, indirectly, when the order parameter is coupled to strain as in ferroelectric and ferromagnetic systems. Shape-memory alloys undergoing a martensitic transition are prototypical systems which display this behavior. In these systems, due to spontaneous symmetry breaking, energetically equivalent domains or variants nucleate at the transition. The arrangement of these domains can be understood as arising from the competition between interface energy (short-range) and long-range interactions arising from compatibility constraints.⁷ In these materials the complexity of the transformation process results in multiscale dynamics characterized by the absence of length and time scales of the transformation events revealed by power-law distributions of the amplitude and duration of AE signals.⁸ This interesting approach to the understanding of the dynamics of the system proves that, in spite of the significant first-order character of

martensitic transitions in shape-memory alloys, some underlying criticality occurs, which is essentially a consequence of the inhomogeneous properties of the material and the long-range correlations between transformation events. Nevertheless, in these AE experiments aimed at statistically analyzing amplitude and duration of AE events, no information regarding the relationship between interface dynamics and AE can be extracted. Actually, it should be possible to obtain this kind of information from the study of AE associated with a propagating parent-martensite interface at constant temperature. We have designed an experiment aimed at exploring this situation as far as possible. This was achieved by inducing the martensitic transition in a Cu-Zn-Al single crystal by controlling the externally applied stress at constant temperature while the strain and AE are measured. Simultaneously, front propagation was observed by means of optical microscopy. Since the transition takes place at (or very close to) the limit of metastability due to its athermal character,⁹ once the parent phase becomes unstable a single variant grows until transformation of the full sample is accomplished. This is essentially different from usual mechanical experiments (performed using standard screw-driven tensile machines) where the controlled variable is the strain. In this case the transition is constrained by the externally imposed length of the sample which prevents free motion of interfaces. In contrast, in our experiment shape changes are not constrained and thus the strain is free to fluctuate. The aim of the present work is studying the relationship between AE and dissipated energy during propagation of martensitic front in a stress-induced transition from cubic to a single-variant martensite.

II. EXPERIMENTAL DETAILS

A single Cu-Zn-Al crystal, obtained by melting metals of 99.999% purity, was grown using a Bridgman technique. Its composition was obtained from energy dispersive x-ray measurements (EDX) to be 68.13 at. % Cu, 15.74 at. % Zn, and

16.13 at. % Al. In the absence of externally applied stress it undergoes a pure structural transition from a cubic ($L2_1$) phase to a martensitic ($18R$) phase at $T_M=234$ K. A rectangular sample with cylindrical heads was machined. The body of the sample had flat faces of 35 mm long (L_s), 3.95 mm wide, and 1.4 mm thick (cross section $\phi=5.53$ mm²). The sample was annealed at 1070 K for 30 min, cooled down to room temperature in air, and finally aged for 2 h in boiling water. The flat surfaces [parallel to the (520) planes] of the sample were mechanically polished to allow *in situ* microscopic observations during loading/unloading experiments.

Stress-controlled experiments have been undertaken within a cryofurnace at a controlled constant temperature of 295.1 ± 0.2 K. We have used a specially designed device which enables fine control of the applied load (a detailed description can be found in Ref. 10). The stress was applied close to the [001] direction of the cubic phase and the trace on the (520) plane of the habit plane of the growing variant was observed to form an angle of $75^\circ \pm 1^\circ$ with the tensile direction. We have checked that, for our specimen, this is the expected angle that is consistent with the phenomenological theory of martensitic transitions.¹¹ Load was increased or decreased at a well-controlled rate by supplying or removing water from a container which was held from the lower grip attached to the sample. The upper grip hung from the ceiling. Acoustic emission was detected by means of a piezoelectric transducer acoustically coupled to the upper grip. The advantage of using piezoelectric sensors is that they are capable of detecting very small events. A number of signals per time interval of 1 s (\dot{N}) with an amplitude exceeding a fixed threshold (used in order to suppress unavoidable noise) were measured with a frequency meter. The length (and thus the deformation) was measured by means of a strain gauge attached to the sample.

III. RESULTS AND DISCUSSION

In Fig. 1 we show, as an example, AE vs applied stress recorded during typical experiments carried out at two selected stress rates. The existence of an intense AE corroborates the jerky character of the dynamics associated with the stress-induced transformation process. Note that a more intense AE activity is detected during the reverse transformation (unloading) than during the forward transformation (loading). This reveals the existence of kinetic differences associated with both forward and reverse transitions. Taking into account that the initial state corresponding to the reverse transition path cannot be properly controlled since different small amounts of parent phase can exist in the system, in the present paper we will only focus on the forward transition. At the same time as AE detection, we have performed *in situ* optical observations which show that martensite nucleates at one of the lateral edges of the sample and grows in the form of needle domains toward the opposite edge. These needle domains belong to the variant which forms an angle of 75° with the tensile direction. Once the first needle domain has reached the opposite edge, cubic-martensite interfaces are created. Further growth of martensite occurs by nucleating new needle domains that propagate parallel to the existing

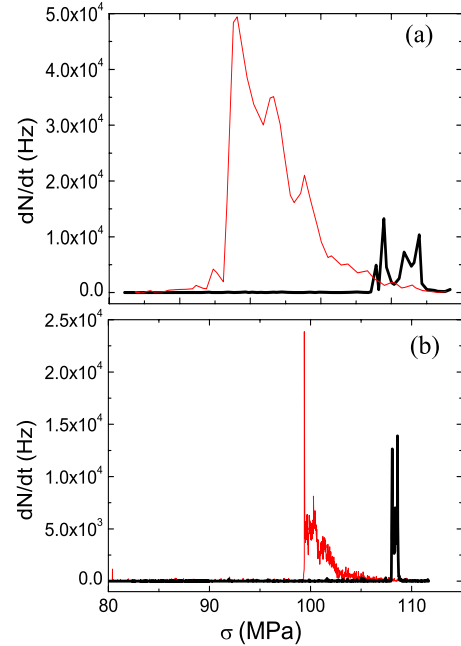


FIG. 1. (Color online) AE activity versus the applied stress during a whole strain-stress cycle. Thicker lines correspond to the loading transition and thinner lines to the unloading reverse transition. The loading rate is $\dot{\sigma}=0.28$ MPa/s in (a) and $\dot{\sigma}=0.01$ MPa/s in (b).

interfaces. We have estimated the thickness of these domains from Fourier analysis of the numerical output from the charge-coupled device (CCD) camera used to record optical images [see Figs. 2(b) and 2(c)]. The estimated thickness is $w \sim 10$ μm . The propagation of these domains shows intermittencies and occurs at high speed. Actually, this discontinuous behavior is responsible for the AE in this process. The transformation mechanism (nucleation and merging of needle domains) gives rise to two fronts propagating in opposite directions at a velocity V [see Figs. 2(a) and 2(b)].

The dynamics of the transformation process is determined by two well separated time scales, a short-time scale associated with needle domains and a long time scale associated

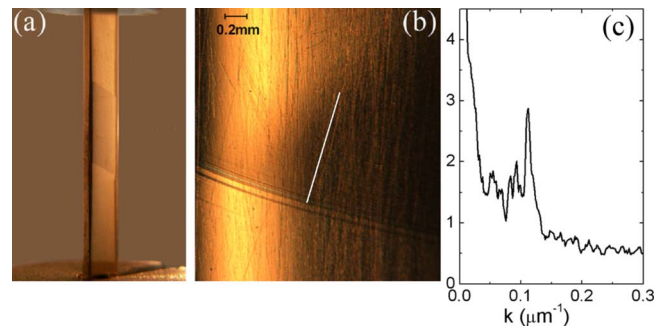


FIG. 2. (Color online) (a) Sample attached to the grips. The transformed region with the two fronts is clearly seen. (b) *In situ* optical observation of one of the propagating fronts. (c) Averaged Fourier transform of the intensity along lines parallel to the white line in (b). From the peak close to $0.1 \mu\text{m}^{-1}$, the thickness of needle domains is estimated to be of the order of $10 \mu\text{m}$.

with front propagation. At this long scale, the front propagation process can be assumed to be continuous in time and can be described by means of a thermodynamic formalism. The transition from the $L2_1$ to the 18R phase is conveniently described by means of a pure strain together with a superimposed modulated displacement.^{12,13} Symmetry arguments allow the Landau free energy to be written as

$$f(\eta, \varepsilon) = \frac{1}{2}A(T)\eta^2 + \frac{1}{4}B\eta^4 + \frac{1}{6}D\eta^6 - \kappa\varepsilon\eta^2 + \frac{1}{2}C\varepsilon^2 - \sigma_t\varepsilon, \quad (1)$$

which includes the coupling of the amplitude η of the modulation (primary order parameter) to the strain ε and the presence of an external stress. In Eq. (1) σ_t is the transformation component of the applied stress σ . The harmonic coefficient is assumed to depend linearly on temperature, $A(T)=a(T-T_c)$. T_c is the limit of stability of the high-temperature phase and C the relevant (soft) elastic modulus. Minimization with respect to ε yields the relationship $\varepsilon=(\kappa\eta^2+\sigma)/C$ between ε and η . Along this (saddle-point) trajectory we obtain an effective free energy,

$$f_{\text{eff}}(\eta) = 1/2[a\{T - [T_c + (2\kappa/aC)\sigma_t]\}\eta^2 + 1/4[B - (2\kappa^2/C)]\eta^4 + 1/6D\eta^6 - \sigma_t^2/2C. \quad (2)$$

We assume that the coupling parameter κ is large enough to ensure that the fourth-order term is negative thus making a first-order transition possible. In this case, the effect of the stress is to shift the equilibrium transition temperature by an amount $\Delta T=(2\kappa/aC)\sigma_t$. It is straightforward to show that $2\kappa/aC=-\Delta S/\Delta\varepsilon$, where ΔS is the transition entropy and $\Delta\varepsilon$ the transformation strain. Next we assume that interface propagation can be described by the following one-dimensional pure relaxational (overdamped) dynamics, $\dot{\eta}=-\Gamma\delta\mathcal{F}/\delta\eta(x)$, where \mathcal{F} is the free-energy functional,

$$\mathcal{F}[\eta(x,t)] = F_0(T) + \int \left[f_{\text{eff}}(\eta) + \frac{1}{2}\mu\left(\frac{\partial\eta}{\partial x}\right)^2 \right] dx. \quad (3)$$

The magnitude of the gradient term, which accounts for the excess of energy associated with the interface, is controlled by the coefficient μ . This approach is expected to be adequate when inertial effects are small as occurs in the low-frequency long-wavelength regime.¹⁴ Moreover, the slowing down effect, which originates from heating effects associated with latent heat dissipation, has also been disregarded. In the steady state, we obtain the following expression for the front velocity of the interface separating both cubic and martensitic phases as expected for a pure relaxational system:¹⁵

$$V \simeq -\Gamma\frac{\mu}{\gamma}\Delta f_{\text{eff}}, \quad (4)$$

where Γ is a mobility, γ is the interface energy, and $-\Delta f_{\text{eff}}$ is the driving force (difference in the free energy between the two homogeneous phases at given values of applied stress and temperature). As ΔS is known to be independent of temperature and stress¹⁶ and $\sigma \ll C\Delta\varepsilon$, the driving force can be expressed as $\Delta\varepsilon(\sigma-\sigma_0)$. σ_0 is the stress at which the transition should occur in equilibrium at temperature T . Note that

$\sigma-\sigma_0$ is a measure of the degree of metastability. Therefore, we expect V to be proportional to the dissipated energy.

On the other hand, at a more microscopic scale, the energy released by the system as AE is known to be proportional to the area slipped by a needle domain.¹⁷ We assume that these domains propagate by steps due to the interaction with defects, such as dislocations. The acoustic signals are proportional to the area swept at each transition step. By considering a rectangular source model, in the far-field approximation, the displacement u_L detected by a transducer at a distance d from the acoustic source is proportional to the velocity of the transformation discontinuity, $u_L \sim v_p(t-\tau)/d$, where τ is the time taken by the wave to reach the transducer and v_p is the velocity of needle domains that at each step propagate much faster than the front ($v_p \gg V$). The number of steps per unit length advanced by the front, λ , is determined by the amount of defects interacting with the domains. Assuming that these defects are homogeneously distributed, the number of AE signals per unit time will simply be given by

$$\dot{N} = \lambda V, \quad (5)$$

which shows [see Eq. (4)] that, within the approximations, the number of AE signals detected per unit time (acoustic emission activity), \dot{N} , must be proportional to the driving force. This is in agreement with the commonly accepted wisdom that AE provides a suitable measure of the dissipated energy associated with the process from which it originates. Note that at each step the velocity of the domain will determine the amplitude of the corresponding AE signal. In order to check the above results we have proceeded as follows. At a constant temperature $T > T_M$, the applied force f and thus the stress ($f = \phi\sigma$) are slowly increased at a rate \dot{f} (or $\dot{\sigma}$), while the macroscopic deformation (relative change in length), $\varepsilon = \delta L/L_s$, and AE are monitored. Once the onset of the transition is reached, f (and thus σ) is kept constant. At this point, $\varepsilon(t)$ is essentially related to the free growth of a single martensitic variant through the propagation of two fronts in opposite directions; the corresponding velocity is given by $V = L_s\dot{\varepsilon}$. In Fig. 3 we show the transition path in stress-strain space. The figure includes the unloading path (performed at a finite rate $-\dot{\sigma}$) so that the whole hysteresis loop is depicted. This hysteresis loop is compared to loops obtained at two finite stress rates. The inset of the figure shows the deformation as a function of time in the transformation region of the loading branch in both $\dot{\sigma}=0$ and $\sigma \neq 0$ cases. When the transformation takes place at constant stress and temperature ($\dot{\sigma}=0$ case), it occurs as a single step. However, as shown in Fig. 4(a) the velocity of the front $V(t)$ is not constant, but rather it fluctuates about an average value $\langle V \rangle$. The velocity corresponding to a situation with $\dot{\sigma} \neq 0$ is plotted in Fig. 4(b). Indeed, the velocity also fluctuates. We have found that the average value of the velocity increases with $\dot{\sigma}$ (see Fig. 5). In the range ΔT from 295 to 310 K [which represents a range of stresses $\Delta\sigma(\simeq\Delta\sigma_0) \simeq \alpha\Delta T$, where $\alpha = \Delta S/\Delta\varepsilon \simeq 2.01$ MPa/K] we have not detected any appreciable dependence of the average velocity on temperature. The observed fluctuations of V with time (in both $\dot{\sigma}=0$ and $\dot{\sigma} \neq 0$ cases) reflect the existence of inhomogeneities

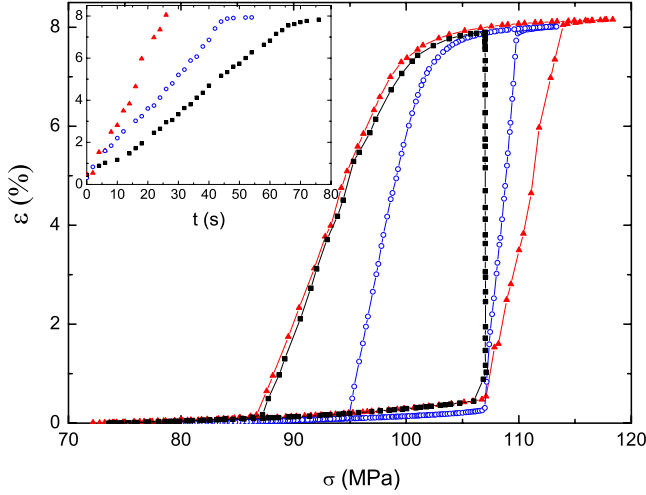


FIG. 3. (Color online) Strain-stress hysteresis loops. For the loop with squares, in the loading branch the stress is kept constant ($\dot{\sigma}=0$) during the transformation (vertical trajectory). For unloading branch the stress is decreased at a rate $\dot{\sigma}=-0.28$ MPa/s. For the loop with triangles, the stress is continuously increased at a rate $\dot{\sigma}=0.28$ MPa/s. It is decreased at rate $\dot{\sigma}=-0.28$ MPa/s in the unloading branch. For the loop with circles the rates are $\dot{\sigma}=0.106$ MPa/s and $\dot{\sigma}=-0.106$ MPa/s in loading and unloading branches. The inset shows the strain as a function of time for the complete forward transformation for the three cases.

in the system which locally modify the degree of metastability. They essentially originate from the same lattice defects that interact with the needle domains and thus this should also be reflected in the behavior of AE. In Figs. 4(a) and 4(b) we have also plotted the AE activity \dot{N} as a function of time for the $\dot{\sigma}=0$ and $\dot{\sigma}\neq 0$ cases, respectively. In both cases, while \dot{N} and $\dot{\epsilon}$ follow the same trend as a function of time, a peak in \dot{N} occurs at the early stages which is not corresponded by a peak in $\dot{\epsilon}$. This behavior is found in most of the experiments performed, and only in a few number of cases, peaks in both quantities are observed. Actually, the lack of coincidence at each time between the AE activity and the strain rate can be explained taking into account that while AE is extremely sensitive to local and rapid changes in the strain field, the strain rate is obtained from a numerical derivative of the measured length change in the full sample (integral and much less sensitive kind of measurement). Comparison of both quantities must be undertaken in a statistical way. We have proceeded by quantifying the similitude of the time dependence of $\dot{N}(t)$ and $\dot{\epsilon}(t)$ by computing the correlation function

$$\zeta = \frac{\langle \dot{\epsilon} \dot{N} \rangle - \langle \dot{\epsilon} \rangle \langle \dot{N} \rangle}{\sqrt{\langle \dot{\epsilon}^2 \rangle - \langle \dot{\epsilon} \rangle^2} \sqrt{\langle \dot{N}^2 \rangle - \langle \dot{N} \rangle^2}} \quad (6)$$

(which takes the value 0 in the absence of correlation and 1 for perfect proportionality) between $\dot{\epsilon}(t)$ and $\dot{N}(t)$. In the inset of Fig. 4(b) we have plotted ζ as a function of $\dot{\sigma}$. It shows that, within errors, the correlation function takes an average value close to 0.6, independent of $\dot{\sigma}$, which is large enough

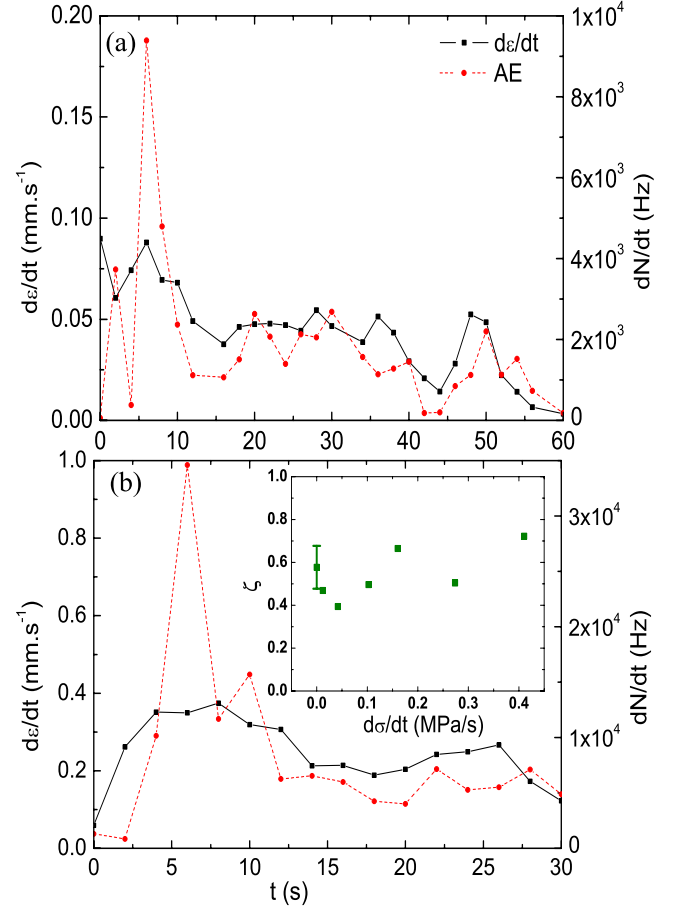


FIG. 4. (Color online) Acoustic emission activity \dot{N} as a function of time (dashed line) compared to the time derivative of the strain $\dot{\epsilon}$ as a function of time (continuous line). The good correlation between the two curves confirms that AE activity is proportional to V . Case (a) corresponds to $\dot{\sigma}=0$ and case (b) to $\dot{\sigma}=0.28$ MPa/s. The inset shows the correlation function between the two curves as a function of the stress rate with a typical error bar indicated.

to corroborate the existence of a reasonably good correlation between the two quantities. Consistently, the average front velocity and the average values of the AE intensity present comparable behavior with increasing $\dot{\sigma}$ (this is shown in Fig. 5). From the results above, the parameter λ [see Eq. (5)] can be estimated to be of the order 10^8 m $^{-1}$. Then, from the sample cross section ϕ and the estimated needle domains thickness w , the density of pinning defects is obtained as $\rho = \lambda w / \phi \approx 5 \times 10^8$ m $^{-2}$. When this value is compared with the density of dislocations in Cu-Zn-Al shape-memory alloys,¹⁸ it is concluded that it represents about 10% of the total amount of dislocations. This result confirms the idea that, to a large extent, pinning effects which give rise to AE mainly originate from dislocations. Furthermore, our results nicely confirm the predicted relationship between measured acoustic emission and dissipated energy. In addition, the increase in the excess of dissipated energy (excess area of hysteresis loops with respect to the loop for which the forward transitions occur at constant σ) as a function of $\dot{\sigma}$ shown in the inset of Fig. 5 provides further support to this conclusion.

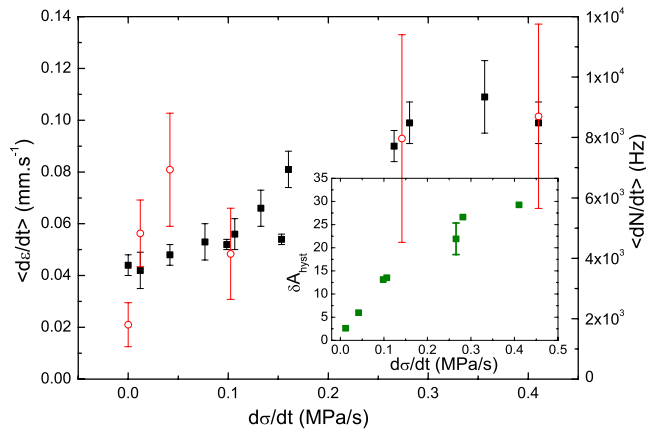


FIG. 5. (Color online) Average values of the time derivative of the strain (proportional to the average velocity $\langle V \rangle$) (solid symbols) and of the AE activity (open symbols) as a function of the stress rate. The error bars are estimations of the standard deviation. The inset shows the excess of dissipated energy as a function of the stress rate with a typical error bar indicated.

IV. SUMMARY AND CONCLUSIONS

To summarize, in the present paper we have shown that AE events during a stress-induced transition to a single-variant martensite are related to the nucleation and propagation of thin needle domains which grow parallel to the transition front. The large number of events (see, for instance, Fig. 1) reflects the jerky character of the propagation dynam-

ics of these needle domains. Actually, this jerky character of the dynamics at this microscopic scale is responsible for the smooth variations of the front velocity. For the overdamped dynamics of the front, the velocity is proportional to the dissipated energy and our results show that it correlates well with time variations of the AE activity. This finding confirms the fact that the AE measured as the number of events per unit time is proportional to the dissipated energy in the transition process. Whether or not there is an underlying criticality related to a critical amount and distribution of disorder, as occurs in temperature-induced martensitic transitions, has not yet been confirmed. As it is known that cycling through the transition modifies the density and distribution of dislocations (defects), we have studied the dependence of ϵ and \dot{N} on the number of transition cycles. As no significant cycling evolution has been found for the free interface propagation, we suggest that no tendency to criticality occurs during the transformation to a single-variant martensite. Self-organization taking place in the multivariant case¹⁹ is thus expected to be a consequence of kinetic constraints during the transformation.

ACKNOWLEDGMENTS

This work has received financial support from CICYT (Spain) under Project No. MAT2007-61200, CIRIT (Catalonia) under Project No. 2005SGR00969, and Marie Curie RTN MULTIMAT (EU) under Contract No. MRTN-CT 2004-5052226.

- ¹D. G. Eitzen and H. N. G. Wadley, J. Res. Natl. Bur. Stand. **89**, 75 (1984).
- ²M. Koslowski, R. LeSar, and R. Thomson, Phys. Rev. Lett. **93**, 125502 (2004).
- ³F. F. Csikor, C. Motz, D. Weygand, M. Zaiser, and S. Zapperi, Science **318**, 251 (2007).
- ⁴S. Zapperi, A. Vespignani, and H. E. Stanley, Nature (London) **388**, 658 (1997).
- ⁵E. Vives, J. Ortín, Ll. Mañosa, I. Ràfols, R. Pérez-Magrané, and A. Planes, Phys. Rev. Lett. **72**, 1694 (1994).
- ⁶M. Roth, E. Mojaev, E. Dul'kin, P. Gemeiner, and B. Dkhil, Phys. Rev. Lett. **98**, 265701 (2007).
- ⁷K. Bhattacharya, *Microstructure of Martensite* (Oxford University Press, New York, 2003).
- ⁸T. Castán, Ll. Mañosa, E. Vives, A. Planes, and A. Saxena, in *Magnetism and Structure in Functional Materials*, edited by A. Planes, Ll. Mañosa, and A. Saxena, (Springer, Berlin, 2005), pp. 27–48.
- ⁹F. J. Pérez-Reche, E. Vives, Ll. Mañosa, and A. Planes, Phys. Rev. Lett. **87**, 195701 (2001).
- ¹⁰E. Bonnot, R. Romero, X. Illa, Ll. Mañosa, A. Planes, and E.

Vives, Phys. Rev. B **76**, 064105 (2007).

- ¹¹C. M. Wayman, *Introduction to the Crystallography of Martensitic Transformations* (MacMillan, New York, 1964).
- ¹²R. J. Gooding and J. A. Krumhansl, Phys. Rev. B **38**, 1695 (1988).
- ¹³A. Planes and Ll. Mañosa, Solid State Phys. **55**, 159 (2001).
- ¹⁴G. S. Bales and R. J. Gooding, Phys. Rev. Lett. **67**, 3412 (1991); T. Lookman, S. R. Shenoy, K. Ø. Rasmussen, A. Saxena, and A. R. Bishop, Phys. Rev. B **67**, 024114 (2003).
- ¹⁵J. S. Langer, in *Solids Far from Equilibrium*, edited by C. Godrèche, (Cambridge University Press, Cambridge, England, 1992), pp. 297–363.
- ¹⁶M. Ahlers, Prog. Mater. Sci. **30**, 135 (1986).
- ¹⁷D. Rouby, P. Fleischman, and C. Duvergier, Philos. Mag. A **47**, 671 (1983).
- ¹⁸W. Salgueiro, R. Romero, A. Somoza, and M. Ahlers, Phys. Status Solidi A **138**, 111 (1993).
- ¹⁹F. J. Pérez-Reche, M. Stípcich, E. Vives, Ll. Mañosa, A. Planes, and M. Morin, Phys. Rev. B **69**, 064101 (2004); F. J. Pérez-Reche, L. Truskinovsky, and G. Zanzotto, Phys. Rev. Lett. **99**, 075501 (2007).